HHS Public Access

Author manuscript

Cancer Lett. Author manuscript; available in PMC 2017 August 23.

Published in final edited form as:

Cancer Lett. 2017 February 01; 386: 141–150. doi:10.1016/j.canlet.2016.11.013.

Adoptive transfer of *ex vivo* expanded Vγ9Vδ2 T cells in combination with zoledronic acid inhibits cancer growth and limits osteolysis in a murine model of osteolytic breast cancer

Aneta Zysk[a], **Mark O. DeNichilo**[a], **Vasilios Panagopoulos**[a], **Irene Zinonos**[a], **Vasilios Liapis**[a], **Shelley Hay**[a], **Wendy Ingman**[b], **Vladimir Ponomarev**[c], **Gerald Atkins**[d], **David Findlay**[d], **Andrew Zannettino**[e], and **Andreas Evdokiou**[a,*]

[a]Discipline of Surgery, Breast Cancer Research Unit, Basil Hetzel Institute, University of Adelaide, Adelaide, South Australia, Australia

[b]Discipline of Surgery, Breast Biology Cancer Unit, Basil Hetzel Institute, University of Adelaide, Adelaide, South Australia, Australia

[c]Department of Radiology, Memorial Sloan-Kettering Cancer Centre, New York, USA

[d]Discipline of Orthopaedics and Trauma, University of Adelaide, Adelaide, South Australia, Australia

[e]School of Medical Sciences, Myeloma Research Laboratory Cancer Theme, South Australian Health and Medical Research Institute (SAHMRI), Faculty of Health Science, University of Adelaide, Australia

Abstract

Bone metastases occur in over 75% of patients with advanced breast cancer and are responsible for high levels of morbidity and mortality. In this study, *ex vivo* expanded cytotoxic Vγ9Vδ2 T cells isolated from human peripheral blood were tested for their anti-cancer efficacy in combination with zoledronic acid (ZOL), using a mouse model of osteolytic breast cancer. *In vitro*, expanded Vγ9Vδ2 T cells were cytotoxic against a panel of human breast cancer cell lines, and ZOL pre-treatment further sensitised breast cancer cells to killing by Vγ9Vδ2 T cells. Vγ9δd2 T cells adoptively transferred into NOD/SCID mice localised to osteolytic breast cancer lesions in the bone, and multiple infusions of Vγ9Vδ2 T cells reduced tumour growth in the bone. ZOL pre-treatment potentiated the anti-cancer efficacy of Vγ9Vδ2 T cells, with mice showing further reductions in tumour burden. Mice treated with the combination also had reduced tumour burden of secondary pulmonary metastases, and decreased bone degradation. Our data suggests that adoptive transfer of Vγ9Vδ2 T cell in combination with ZOL may prove an effective immunotherapeutic approach for the treatment of breast cancer bone metastases.

*Corresponding author. Breast Cancer Research Unit, Level 1, Basil Hetzel Institute, Queen Elizabeth Hospital, 28 Woodville Road, Woodville, South Australia, Australia. Fax: +61 8 8222 7451. andreas.evdokiou@adelaide.edu.au (A. Evdokiou).

Conflict of interest

The authors declare no conflict of interest.

Keywords

Metastasis; Immunotherapy; Bisphosphonate; Osteoclast; Tumour associated macrophage

Introduction

Breast cancer is one of the most commonly diagnosed cancers in women worldwide. Patients diagnosed with primary breast cancer have higher survival rates compared to those diagnosed with the advanced disease, primarily due to cancer metastases [1]. Bone metastases occur in over 75% of patients with advanced breast cancer, resulting in extensive bone degradation leading to skeletal-related events (SREs) such as hypercalcemia, chronic pain, fracture, spinal cord compression, and impaired mobility, all which greatly affect quality of life [2,3]. Breast cancer bone metastases are predominately osteolytic due to factors secreted by disseminated tumour cells that stimulate osteoclasts [4]. Activated osteoclasts degrade bone and release growth factors from the matrix that further promote tumour growth and bone destruction, perpetuating the 'vicious cycle' of cancer growth and bone destruction [5]. Nitrogen-containing bisphosphonates (nBPs), a class of anti-resorptive drugs, are currently used to inhibit osteoclast-mediated bone degradation in patients with skeletal malignancies, including advanced breast cancer, however, this treatment is only palliative and new therapeutic approaches are required [6,7].

Within the past decade, immunotherapy of cytotoxic gamma delta (γδ) T cells has been gaining momentum as a potential therapeutic approach for targeting cancer. Human γδ T cells comprise a small population (1–10%) of circulating peripheral blood lymphocytes [8]. These primarily consist of the V52 chain in combination with Vγ9(Vγ9Vδ2) which are stimulated and expanded in response of phosphoantigens (PAgs).

Activated Vγ9Vδ2 T cells have the ability to recognise target cells in an MHC-unrestricted manner [9] via detection of PAgs, including isopentenyl pyrophosphate (IPP), an intermediate of the mammalian mevalonate pathway. nBPs, including zoledronic acid (ZOL) inhibit the mevalonate pathway resulting in IPP accumulation which activate and expand Vγ9Vδ2 T cells [10–16].

Due to abnormal upregulation of the mevalonate pathway, tumour cells accumulate PAgs resulting in recognition by Vγ9Vδ2T cells [17]. Activated Vγ9Vδ2 T cells can then kill cancer cells by releasing Th1 cytokines, including TNF-α (tumour necrosis factor-alpha) and IFN-γ (interferon-gamma) [18–20] and cytolytic granules [10,19–21].Vγ9Vδ2 T cells also induce target cell death by death receptor/ligand interactions with TRAIL (Apo2L) [21], and FASL (Fas ligand) [11]. As a result, expanded Vγ9Vδ2 T cells exert potent cytotoxicity against a variety of solid and haematological malignancies, *in vitro* and in vivo [10–12,15,22,23].

Vγ9Vδ2 T cell immunotherapy has been assessed against a variety of solid and haematological malignancies in early phase clinical trials (reviewed in Ref. [24]). While these trials have deemed Vγ9Vδ2 T cell therapy safe, as a monotherapy the anti-cancer efficacy, especially against advanced tumours has been underwhelming and requires further

improvement. In addition to activating Vγ9Vδ2 T cells, ZOL can also sensitise cancer cells to killing by Vγ9Vδ2 T cells both in *vitro* and in vivo [13–15,21,25]. Additionally, clinical evidence demonstrates the potential of using Vγ9Vδ2 T cell adoptive transfer in combination with ZOL for the treatment of advanced renal cell carcinoma (RCC), malignant ascites from gastric cancer, and other metastatic tumours [26–28].

As ZOL preferentially localises to the bone, an elegant approach for targeting cancer lesions in the bone has emerged. Discussion in the literature have suggested that nBP administration followed by adoptive transfer of Vγ9Vδ2 T cells would be an ideal two-pronged approach for targeting cancers in the bone [29]. This immunotherapy would allow simultaneous reduction of tumour-associated bone loss in addition to sensitising cancer cells to Vγ9Vδ2 T cell mediated cytotoxicity, inhibiting the vicious cycle of bone destruction and cancer growth. To date, adoptive transfer of Vγ9Vδ2 T cells alone or in combination with ZOL to specifically target cancers in the bone has not been fully investigated. In this study, we used a murine model of osteolytic breast cancer, where breast cancer cells were implanted directly into the tibia in NOD/SCID mice. We showed for the first time, that Vγ9Vδ2 T cells localised to osteolytic breast cancer lesions growing in the bone and that multiple infusions of Vγ9Vδ2 T cells slowed tumour growth. We also showed that ZOL potentiated the anti-cancer efficacy of Vγ9Vδ2 T cells, decreased tumour burden in the bone, inhibited tumour-associated osteolysis, and decreased lung metastases tumour burden.

Materials and methods

Cells and reagents

ZR75 and T47D human breast cancer cell lines were obtained from American Type Culture Collection. The MDA-MB231 human breast cancer derivative cell line MDA-MB231-TXSA was kindly provided by Dr. Toshiyuki Yoneda (University of Texas Health Science Centre, San Antonio, Texas). MDA-MB231-TXSA expressed GFP and luciferase produced by retroviral expression of the SFG-NES-TGL vector, as previously described [30]. All cell lines were cultured in DMEM (Life Technologies, Australia) supplemented with 10% foetal bovine serum (FBS, Life Technologies, Australia), 100 IU/mL penicillin (Life Technologies, Australia), 100 μg/mL streptomycin (Life Technologies, Australia), and 25 mM HEPES (Life Technologies, Australia) at 37°C in a 5% CO_2 humidified atmosphere. ZOL was generously provided by Novartis Pharma AG.

Ex vivo expansion of Vγ9Vδ2 T cells

Informed consent was obtained prior to collection of peripheral blood from healthy adult donors. PBMC were isolated immediately via density gradient centrifugation using Lymphoprep™ (Axis Shield, Norway) following manufacturer's instructions. PBMCs were resuspended to 1×10^6/mL in CTS™ OpTmizer™ T Cell Expansion SFM (Life Technologies, Australia) supplemented with OpTmizer™ T cell Expansion Supplement (1:38 dilution) (Life Technologies, Australia), 10% heat-inactivated FBS (HI-FBS), 100 IU/mL penicillin, 100 μg/mL streptomycin, 2 mmol L-glutamine (Life Technologies, Australia), 25 mM HEPES, 0.1% β-mercaptoethanol (Sigma–Aldrich, USA), 100 IU/mL recombinant human interleukin 2 (rhIL-2) (BD Pharmingen, USA) and activated with 5 μM

ZOL, and seeded into 6-well plates. Cell culture density was maintained at 1–2 × 10^6 cells/mL and replenished with fresh medium containing 100 IU/mL rhIL-2 only (without ZOL) every 2–3 days. Following 7–8 days of culture cells were collected and enriched as described below.

Enrichment of Vγ9Vδ2 T cells

Ex vivo expanded Vγ9Vδ2 T cells were enriched prior to *in vitro* and *in vivo* experiments using negative selection MACS with the TCR γ/δ+ T cell Isolation Kit (human) (Miltenyi Biotec, Germany). Cell viability and total cells numbers after enrichment were assessed using trypan blue exclusion. Percentage of Vγ9Vδ2 T cells were determined by flow cytometry using PeCy5 conjugated anti-CD3 (clone UCHT1) (eBioscience, San Diego, CA, USA) and FITC conjugated anti-Vγ9 TCR from BD Biosciences (San Jose, CA, USA). Analysis was performed on the BD FACSCanto II Flow Cytometer (San Jose, CA, USA). Percentages of Vγ9Vδ2 T cells were identified by gating on the lymphocyte population using forward scatter/side scatter then on $Vγ9^+$ $CD3^+$ double positive cells. After enrichment, Vγ9Vδ2 T cell viability was >95%, and the percentage of Vγ9Vδ2 T cells was consistently >97%.

Cell cytotoxicity assay

Cytotoxicity of Vγ9Vδ2 T cells against breast cancer cell lines was assessed using a standard lactate dehydrogenase (LDH) release assay (CytoTox 96® Non-Radioactive Cytotoxicity Assay; Promega, USA). Briefly, 1 × 10^4 target cells were seeded in triplicate in a 96-well microtiter plate and allowed to adhere overnight. Target cells were then treated with or without 25 μM ZOL for 24 h, and then co-cultured with Vγ9Vδ2 T cells at 1:1,5:1 and 10:1 effector:target (E:T) ratio, with Vγ9Vδ2 T cells as the effector, and cancer cells as the target. After incubation for 9 h at 37°C, 50 μLof supernatant was assayed for LDH activity following the manufactures protocol. The appropriate controls were prepared and cytotoxicity was calculated as:

$$\%\ Cytotoxicity = \frac{experimental\ release - \ effector\ spontaneous\ release - \ target\ spontaneous\ release}{targetmaximumrelease - targetspontaneousrelease} \times 100$$

Cell viability assay

MDA-MB231-TXSA cells expressed luciferase, which was the basis for a luciferase activity viability assay using Dual Luciferase® Reporter Assay kit (Promega, Madison, WI, USA). Briefly, 1 × 10^4 luciferase-tagged target cells were seeded in triplicate in a 96-well microtiter plate and allowed to adhere overnight. Cells were then treated with or without 25 μM ZOL for 24 h, and then co-cultured with Vγ9Vδ2 T cells at 1:1,5:1 and 10:1 E:T ratios. After 24 h incubation, media was removed and cells were washed in PBS, then lysates were prepared and analysed following the manufacturers protocol. Viability was calculated as:

$$\%\ Viability = \frac{experimental\ value}{untreated\ control\ value} \times 100$$

Measurement of DEVD-caspase activity

DEVD-caspase activity was assayed by cleavage of zDEVD-AFC (z-asp-glu-val-asp-7-amino-4-trifluoro-methyl-coumarin), a fluorogenic substrate based on the peptide sequence at the caspase-3 cleavage site of poly (ADP-ribose) polymerases (Kamiya Biomedical Company, Seattle, WA, USA). Breast cancer cells were seeded at 1×10^4 cells/well in triplicate a 96-well microtiter plate and allowed to adhere overnight. Cells were then treated with or without 25 μM ZOL for 18 h, then co-cultured with Vγ9Vδ2 T cells at a 5:1 E:T ratio for 2 h. Caspase activation was detected using DEVD-AFC, as previously described in [31].

Western immunoblotting

Detection of unprenylated small GTPases, including RAP1, were used to indirectly determine the extent of FPPS inhibition by ZOL, which correlates with increased IPP levels, resulting in the increased detection of cancer cells by Vγ9Vδ2 T cells and greater cytotoxicity. To determine the effect of ZOL on the prenylation of small GTPases in the breast cancer cells, lysates were analysed by Western immunoblotting for total and unprenylated RAP1. Briefly, $1 \chi 10^6$ breast cancer cells were seeded in a 25-cm^2 flask, allowed to adhere, and then treated with 25 μM ZOL for 18 h or over a 24 h time course. Lysates were prepared and separated as previously described [31] and immunodetection was performed overnight at 4°C in PBS/blocking reagent containing 0.1% Tween-20, using the following primary antibodies at the dilutions suggested by the manufacturer: pAb anti-RAP1 (121) for total RAP1 protein, pAB anti-RAP1A (C-17) specifically for unprenylated RAP1 (Santa Cruz Biotechnology, USA), and anti-actin mAb (Sigma–Aldrich, USA) as a loading control. Membranes were then rinsed several times with PBS containing 0.1% Tween-20 and incubated with 1:5000 dilution of anti-goat or anti-rabbit alkaline phosphatase-conjugated secondary antibodies (Thermo Fisher Scientific, USA) for 1 h. Visualisation of protein bands was performed using the ECF substrate reagent kit (GE Healthcare, UK) on a LAS-4000 (GE Healthcare, UK).

Labelling Vγ9Vδ2 T cells with DiR

Vγ9Vδ2 T cells were expanded *ex vivo* and enriched as described above, washed in PBS, and resuspended to $2 \chi 10^6$ cells/mL in RPMI-1640 media (Life Technologies, Australia) supplemented with 0.1% HI-FBS. XenoLight DiR Fluorescent Dye (Perkin Elmer, USA) was reconstituted in ethanol and added to cells at a final concentration of 16.6 μg/mL. Cells were incubated in the dark for 10–15 min at 37°C, then collected and washed three times in PBS containing 1% HI-FBS. Cell viability was assessed using trypan blue exclusion; labelling efficacy was assessed by flow cytometry using the filter corresponding to PeCy7; and cytotoxicity was assessed using the DEVD-Caspase assay, as outlined above.

Animals

Female four-week-old non-obese diabetic severe combined immunodeficient (NOD/SCID) mice were purchased from the Animal Resources Centre (Canning Vale, WA, Australia) and housed under pathogen free conditions in The Queen Elizabeth Hospital Experimental Surgical Suite (Woodville, SA, Australia). Mice were acclimatised to the animal housing

facility and the general wellbeing of animals was monitored continuously throughout the experiment. All experimental procedures were carried out with strict adherence to the rules and guidelines for the ethical use of animals in research and were approved by the Animal Ethics Committees of the University of Adelaide and the Institute of Medical and Veterinary Science, Adelaide, SA, Australia.

In vivo fluorescence and bioluminescence imaging

Non-invasive, whole body imaging to monitor DiR-labelled Vγ9Vδ2 T cell localisation and luciferase-tagged MDA-MB231-TXSA cancer cell growth *in vivo* was performed on the IVIS Spectrum *in vivo* Imaging system (Caliper Life Sciences, Australia). For fluorescence imaging, mice were anaesthetised by isoflurane (Veterinary Companies of Australia, Australia) and fluorescence images were acquired using the optimised settings for DiR dye: f stop: 2, medium binning, ex/em: 745/800 nm. Images were taken at multiple time points, up to 120 s. For bioluminescence imaging, mice were injected s.c with 100 μL D-luciferin solution (Perkin Elmer, USA) to a final dose of 3 mg/20 g mouse body weight and then anaesthetised by isoflurane. Bioluminescence was acquired between 0.5 and 30 s (representative images shown at 1 s). Photon emission was quantified as Total Flux measured in [photons/second] using Living Image 4.2 (Caliper Life Sciences, Australia). There was no interference between the DiR dye and the luciferase-tagged cancer cells, therefore fluorescence and bioluminescence images could be acquired in succession to assess Vγ9Vδ2 T cell localisation.

Intratibial injections of breast cancer cells

Intratibial (i.t) injections were performed as previously described [30]. Briefly, five-week old female NOD/SCID mice were anaesthetised by isoflurane (Veterinary Companies of Australia, Australia). The left leg was shaved, then wiped with 70% ethanol and a 27-guage needle coupled to a Hamilton syringe was used to inject luciferase-tagged MDA-MB231-TXSA (1×10^5 cells) resuspended in 10 μL PBS through the tibial plateau into the marrow space. The contralateral tibia was not injected.

In vivo localisation

I.t injections were performed as described above, and once tumour were established, mice were injected 5×10^6 DiR-labelled Vγ9Vδ2 T cells i.v (n = 5). Fluorescence and bioluminescence images were acquired as described above after 20 min, 1 h, 24 h and 6 days.

In vivo anti-cancer efficacy of ZOL and Vγ9Vδ2 T cells

I.t injections were performed as described above and two days post inoculation, tumour growth was assessed by bioluminescence imaging using the IVIS Spectrum. When tumours were established, mice were assigned into four treatment groups (n = 4–6): control, ZOLalone (100 μg/kg s.c), Vγ9Vδ2 T cells alone (1×10^7 Vγ9Vδ2T cells injected i.v via the tail vein), and ZOL in combination with Vγ9Vδ2 T cells (infusion of Vγ9Vδ2 T cells 24 h after ZOL, treatments as above). If pain relief was required, Rimadyl (carprofen) (Pfizer Animal Health, Australia) was administered at 5 mg/kg s.c every 24 h for a

maximum of three days. After 3 weeks treatment, mice were sacrificed and the tumour bearing and non-tumour bearing tibia from each animal were surgically resected for micro-computed tomography (μCT).

Ex vivo micro-computed tomography (μCT) analysis

Tibias for μCT analysis were scanned using the SkyScan-1076 high-resolution μCT Scanner (Bruker). The scanner was operated at 50 kV, 110 μA, rotation step of 0.5, 0.5-mm aluminium filter, and scan resolution of 7.8 μm/pixel. Cross-sections were reconstructed using the cone-beam algorithm in NRecon (V1.6.9.8, Bruker). Images were then realigned in DataViewer (1.5.1.2, Bruker) and imported into CT Analyser (CTAn) (V1.14.4.1+, Bruker, Skyscan). Using the two-dimensional images obtained from the CTAn, the growth plate was identified and 600 sections starting from the growth plate/tibial interface and moving down the tibia were selected for quantification of total bone morphometric parameters and 200 sections starting 25 sections down from the growth plate, were selected for trabecular bone morphometric parameters. Representative three-dimensional images were generated in CTvox (V2.7.0, Bruker).

Histology

Tibias were fixed in 10% buffered formalin, followed by 6 weeks decalcification in 0.5 M EDTA/0.5% paraformaldehyde in PBS, pH 8.0 at room temperature. Complete decalcification was confirmed by radiography and tibias were then paraffin embedded and sectioned longitudinally at 6 μm. Osteoclast-specific tartrate-resistant acid phosphatase (TRAP) staining was conducted following the manufacturer's protocol (386A, Sigma Aldrich). Slides were then imaged using Nanozoomer-HT Digital Pathology (NDP, Hamamatsu) and photos were acquired at 4x and 40x magnification using Nanozoomer software NDP.view (V1.2.33, Hamamatsu). Osteoclast number was determined by counting TRAP positive multi-nucleated (≥3 nuclei) cells in a 1 mm^2 area below the growth plate.

Data analysis and statistics

In vitro experiments were conducted at least twice using biological triplicates, and data presented is mean ± SEM, unless otherwise specified. A representative experiment is shown for Western immunoblot data. Two-tailed unpaired Student's t-test was used and in all cases p-values <0.05 were considered statistically significant. All statistical analysis was conducted using SigmaPlot v12.5 (Systat Software Inc., USA).

Results

ZOL sensitises breast cancer cells to Vγ9Vδ2 T cell cytotoxicity in vitro

The cytotoxicity of purified *ex vivo* expanded Vγ9Vδ2 T cells alone and in combination with ZOL was first evaluated against a panel of human breast cancer cell lines. MDA-MB231-TXSA showed cytotoxicity in an E:T dependent manner after 9 h co-culture with Vγ9Vδ2 T cells alone (maximum 28% specific lysis), while T47D and ZR75 cells were relatively resistant. However, after 24 h pre-treatment with ZOL followed by 9 h co-culture with Vγ9Vδ2T cells, there was a significant increase in cytotoxicity in each cell line which occurred in an E:T dependent manner, resulting in a maximum of 18% (ZR75), 50% (T47D)

and 80% (MDA-MB231-TXSA) specific lysis (Fig. 1A). Co-culture of each cell line with Vγ9Vδ2 showed a small but statistically significant increase in caspase-3 activation, with the MDA-MB231-TXSA cells showing a 2-fold increase in caspase-3 activation after Vγ9Vδ2 T cells alone (Fig. 1B). However, after 24 h pre-treatment with ZOL then 2 h co-culture with Vγ9Vδ2 T cells, each cell line except ZR75, showed significantly higher caspase-3 activation compared to Vγ9Vδ2 T cells alone. T47D and MDA-MB231-TXSA showed a 1.7 and 5.3-fold increase in caspase-3 activation respectively (Fig. 1B).

To determine possible reasons for the differential sensitivity to Vγ9Vδ2 T cells after ZOL pre-treatment between the three breast cancer cell lines, we examined inhibition of RAP1 prenylation (a surrogate marker for inhibition of the mevalonate pathway) after 18 h of ZOL treatment using Western immunoblot analysis. This method was used to indirectly determine the extent of FPPS inhibition by ZOL, which leads to increased IPP levels, potentially resulting in the increased detection of cancer cells by Vγ9Vδ2 T cells and greater cytotoxicity. After 18 h pre-treatment with 25 μM ZOL, MDA-MB231-TXSA showed an increase in unprenylated RAP1 compared to untreated control (Fig. 1C), while ZR75 and T47D showed no detectable unprenylated RAP1 compared to untreated. A time course analysis of MDA-MB231-TXSA treated with 25 μM ZOL, showed unprenylated RAP1 was detectable as early as one hour post treatment and peaked at 24 h (Fig. 1D).

Since MDA-MB231-TXSA were consistently the most sensitive breast cancer cell line to Vγ9Vδ2 T cell cytotoxicity, further experiments were conducted to establish an optimal time course for Vγ9Vδ2 T cell cytotoxicity after ZOL pre-treatment. A luciferase-based activity assay was used to determine the viability of cancer cells after 24 h pre-treatment with or without 25 μM ZOL followed by co-cultured with Vγ9Vδ2 T cells for 4 or 24 h. After a 4 h co-culture, Vγ9Vδ2 T cells alone did not reduce MDA-MB231-TXSA viability, however, pre-treatment with ZOL greatly enhanced Vγ9Vδ2 T cell cytotoxicity, resulting in a significant decrease MDA-MB23-TXSA viability in an E:T dependent manner (maximum 46% viable) (Fig. 2A). In contrast, after a 24 h co-culture with Vγ9Vδ2T cells in the absence of ZOL, an E:T dependent decrease in cancer cell viability (maximum 60% viable) was observed (Fig. 2B). Pre-treatment of MDA-MB231-TXSA with ZOL further potentiated the cytotoxicity of Vγ9Vδ2 T cells resulting in almost 100% death of cancer cells at all E:T tested (Fig. 2B).

Adoptively transfered Vγ9Vδ2 T cells localise to breast cancer lesions in the bone

To date, no studies have demonstrated localisation of Vγ9Vδ2T cells to tumours in the bone. To examine the potential for Vγ9Vδ2T cells to co-localise with tumours in the bone microenvironment, a near infrared dye (DiR) was used to fluorescently label Vγ9Vδ2T cells for live *in vivo* imaging. We established a protocol that allowed consistent labelling of Vγ9Vδ2 T cells, with a labelling efficiency of >80% as analysed by flow cytometry (Fig. 3A). Labelling Vγ9Vδ2T cells with the fluorescent dye had no effect on the viability of Vγ9Vδ2 T cells (data not shown), or on their ability to induce cell death of MDA-MB231-TXSA cancer cells, compared to unlabelled Vγ9Vδ2 T cells (Fig. 3B). For localisation studies, mice were inoculated with luciferase-tagged MDA-MB231-TXSA cancer cells directly into the bone marrow cavity of the left tibia. After one week, tumours were

established as measured by bioluminescence signal from the tibia. Fluorescently labelled Vγ9Vδ2 T cells were injected intravenously into the animals. Within 20 min of infusion, fluorescence signal was detected only in the lungs and liver (data not shown). However, after 24 h, a strong fluorescence signal was also detected in the tumour bearing tibia, corresponding to areas of tumour bioluminescence (Fig. 3C). At this time, fluorescence in the lungs diminished, whereas the fluorescence signal persisted in the liver until the end of the study, six days later. Overall, the fluorescence signal progressively declined over the next six days, at which point, mice were sacrificed and tibias were imaged *ex vivo*. Mice showed fluorescence which corresponded to areas of tumour bioluminescence in the tumour bearing tibias (Fig. 3D), as well as fluorescence in the liver and spleen, which has been previously reported with adoptive transfer of Vγ9Vδ2 T cells [23,32].

ZOL potentiates the anti-cancer efficacy of Vγ9Vδ2 T cells against osteolytic breast cancer and reduces tumour burden of lung metastases

We next examined the *in vivo* efficacy of *ex vivo* expanded Vγ9Vδ2 T cells in a model of osteolytic breast cancer. Mice were inoculated with luciferase-tagged MDA-MB231-TXSA cells directly into the left tibia of mice. Treatments were initiated once tumours had established, as measured by bioluminescence imaging. Animals were pre-treated with ZOL 24 h prior to Vγ9Vδ2 T cell adoptive transfer. This treatment regime was repeated three times over two weeks. Animals treated with ZOL alone had no effect on tumour burden when compared to untreated animals (Fig. 4). A trend showing decreased tumour growth, which did not reach statistical significance, was observed in animals adoptively transferred with Vγ9Vδ2 T cells alone compared to untreated control or ZOL alone treated animals. In contrast, pre-treatment with ZOL, followed by adoptive transfer of Vγ9Vδ2 T cells, potentiated the anti-cancer efficacy of Vγ9Vδ2 T cells. These animals showed the smallest tumours of all treatment groups, which was evident after the third infusion dose of Vγ9Vδ2 T cells. Additionally, Vγ9Vδ2 T cells in combination with ZOL reduced pulmonary tumour burden in those animals that developed lung metastases, compared to animals in the untreated control or ZOL alone treated groups (Fig. 5).

ZOL in combination with Vγ9Vδ2 T cells reduces tumour-induced osteolysis

MDA-MB231-TXSA breast cancer cells growing within the bone give rise to predominantly osteolytic lesions [30,33]. To evaluate the ability of Vγ9Vδ2 T cells alone or in combination with ZOL to protect the bone from tumour-induced osteolysis, tibias were analysed using three-dimensional (3D) μCT imaging and TRAP staining of bone sections was used to visualise and quantify $TRAP^+$ osteoclasts.

Osteolysis was measured as a net loss of total bone volume (T.BV) and trabecular bone volume (Tb.BV) by comparing the tumour bearing tibia to the contralateral non-tumour bearing tibia of the same animal. Qualitative and quantitative μCT showed bone loss in all groups, but with notable differences in the extent of osteolysis (Fig. 6A). Animals that remained untreated showed the greatest osteolysis, with a net loss T.BV of 16% compared to the contralateral non-tumour bearing tibia. As expected, ZOL treatment reduced the extent of osteolysis, to 7% T.BV. Vγ9Vδ2 T cells alone only marginally reduced the T.BV from 16% to 11%. In contrast, treatment with ZOL in combination with Vγ9Vδ2 T cells showed

an additive effect in reducing osteolysis, with total BV loss of only 4%. Tb.BV loss was more profound in all treatment groups (Fig. 6B). Animals in the untreated group had a Tb.BV loss of 87%, Vγ9Vδ2 T cells alone increased Tb.BV loss to 65% and ZOL treatment alone increased Tb.BV loss to 49%. ZOL in combination with Vγ9Vδ2 T cells had the least Tb.BV loss at 27%.

Untreated animals showed abundant $TRAP^+$ osteoclasts lining the bone surface, in contrast to animals treated with ZOL alone or ZOL in combination with Vγ9Vδ2 T cells (Fig. 6C). Animals treated with ZOL alone showed a significant decrease in $TRAP^+$ osteoclasts compared to untreated animals (Fig. 6D). A trend showing reduced osteoclast number was observed in the Vγ9Vδ2 T cell alone treated group, however this did not reach statistical significance (Fig. 6D). Furthermore, there were no significant differences in osteoclast number between animals treated with ZOL alone and ZOL in combination with Vγ9Vδ2 T cells (Fig. 6D), suggesting that ZOL alone was responsible for the observed decrease in osteoclasts in the combination treatment group.

Discussion

In this study, we used a well-established murine model of osteolytic breast cancer to examine the anti-cancer efficacy of adoptively transferred *ex vivo* expanded Vγ9Vδ2 T cells alone and in combination with ZOL. The MDA-MB231 derivative cell line, MDA-MB231-TXSA, is a highly osteolytic breast cancer cell line which mimics abnormal osteoclast-mediated bone degradation commonly seen in breast cancer bone metastases [30,33]. *In vitro* pre-treatment of MDA-MB231-TXSA with ZOL lead to a significant augmentation of Vγ9Vδ2 T cell mediated cytotoxicity, which was associated with a time-dependent inhibition of RAP1 prenylation, a surrogate marker of the mevalonate pathway. However, not all breast cancer cell lines were sensitised to Vγ9Vδ2 T cells following ZOL pre-treatment. Observed differences may arise from the ability of cells to uptake nBPs, which varies depending on cell type, and on mevalonate pathway activity [15,34]. Following ZOL pre-treatment, MDA-MB231-TXSA showed the greatest inhibition of RAP1 prenylation, suggesting the sensitivity of cancer cells to killing by Vγ9Vδ2 T cells after ZOL pre-treatment correlated with the accumulation of intracellular PAgs after exposure to ZOL.

In vivo, we have demonstrated for the first time that adoptively transferred Vγ9Vδ2 T cells localised to tumours in the tibia and persisted for up to 6 days following infusion. This is consistent with previous findings in other soft tissue tumours including breast and prostate cancer demonstrating the ability of Vγ9Vδ2 T to localise to tumour lesions [23,32]. Adoptively transferred Vγ9Vδ2 T cells were also observed in the liver. When a substance is injected intravenously via the tail vein, it is directly delivered to the liver, which accounts for this observation.

When Vγ9Vδ2 T cells were infused alone, there was minimal reduction in tumour burden in the bone. However, pre-treatment of mice with ZOL greatly potentiated the anti-cancer efficacy of adoptively transferred Vγ9Vδ2 T cells against tumour growth in bone and also considerably reduced pulmonary metastases burden. This decrease in lung metastases is

consistent with similar observations in both pre-clinical studies in prostate cancer [35] and early phase clinical trials in patients with advanced renal cell carcinoma [26].

Given the well-characterised effects of ZOL on the mevalonate pathway and our *in vitro* observations showing inhibition of RAP1 prenylation, our data suggest that cellular accumulation of IPP caused by inhibition of FPPS establishes greater recognition and targeting of cancer cells by Vγ9Vδ2 T cells. Benzaid et al. demonstrated that mice treated with ZOL showed IPP accumulation in mammary fat pad tumours [15]. Additionally, mice that were infused with human PBMC in combination with ZOL and IL-2 showed *in vivo* expansion of Vγ9Vδ2 T cells, and treatment inhibited tumour growth, compared to untreated animals and those treated with ZOL alone or PBMC + IL-2, with the authors' suggesting cancer cells could internalise ZOL *in vivo* [15]. However, following ZOL administration there is a transient peak followed by rapid clearance of ZOL with its permanent retention in bone, thus it is not available for internalisation by cancer cells resident in the bone marrow. Additionally, using real-time intravital imaging within mammary fat pad tumours, Junankar et al. recently showed that fluorescently labelled nBPs were not internalise by cancer cells, but rather by tumour associated macrophages (TAMs) [36], suggesting IPP accumulation within the tumour mass would arise from the TAM population. Macrophages and osteoclasts are derived from the same lineage and both internalise ZOL via fluid-phase endo-cytosis [37]. Within the bone, osteoclasts and monocytes uptake nBPs [38], therefore it is reasonable to suggest that within the bone tumour microenvironment, these cells uptake ZOL and cancer cells do not. Previously, Ferrero et al. reported that *mycobacterium tuberculosis* pulsed macrophages produce monocyte chemoattractant protein-1 (MCP-1) and IL-8, which promote chemotaxis of γδ T cells *in vitro* [39]. CCR2, a receptor for MCP-1, is expressed on activated Vγ9Vδ2 T cells [20] suggesting that macrophages and/or osteoclasts which have internalised ZOL may attract activated Vγ9Vδ2 T cells to the tumour microenvironment resulting in greater anti-cancer efficacy. However, further studies are required to examine the underlying mechanisms of ZOL sensitisation *in vivo*.

nBPs are well-characterised anti-bone resorptive agents, additionally, they are reported to induce cancer cell death, inhibit proliferation, invasion, and angiogenesis *in vitro* [40–45]. However, the current literature surrounding ZOL *in vivo* anti-cancer efficacy is still contradictory [46–51]. In this current study, frequent ZOL administrations inhibited cancer-associated bone loss, however there was no effect on tumour burden. These findings are consistent with previous studies from our laboratory using an intratibial model of orthotropic osteosarcoma [50,51]. Interestingly, more frequent ZOL administrations at a lower dose (metronomic dosing), were previously shown to inhibit both tumour growth and protect the bone from tumour-associated osteolysis [48] indicating further *in vivo* optimisation to reduce tumour growth in this model may be required.

In contrast to the well-known anti-bone resorptive effects of ZOL, the effect Vγ9Vδ2 T cells have on bone is still unclear. The first indication that Vγ9Vδ2 T cells may contribute to osteoimmunology was the correlation observed between Vγ9Vδ2 T cell depletion and the incidence of bisphosphonate-associated osteonecrosis of the jaw in osteoporotic patients treated with intravenous nBPs [52].In this current study, Vγ9Vδ2 T cells alone marginally

inhibited tumour-associated bone loss; however, the mechanisms by which this occurs is still unclear. Previous *in vitro* studies demonstrated that activated donor-matched human γδ T cells inhibit osteoclast formation from PBMC [53] and Vγ9Vδ2 T cells are cytotoxic towards osteoclasts in co-culture with multiple myeloma cells [12]. Targeting osteoclasts would result in increased bone volume, as observed in this current study. Vγ9Vδ2 T cells also have the potential to produce IGF-1 and low levels of FGF-2 following antigen stimulation [54]. IGF and FGF are osteoblast growth factors, suggesting that if Vγ9Vδ2 T cells are primed to produce these factors following localisation to the bone, in addition to their potential cytotoxicity against osteoclasts, they could stimulate new bone resulting in a net gain in bone volume. As Vγ9Vδ2 T cells also target cancer cells, they may have an indirect effect on bone loss by reducing tumour growth and subsequently inhibiting the 'vicious cycle'.

Collectively, this study demonstrates that *ex vivo* expanded Vγ9Vδ2 T cells readily localise to osteolytic breast cancer lesions in the bone and exhibit some anti-cancer efficacy, which is enhanced following ZOL pre-treatment. Our data suggests that adoptive transfer of Vγ9Vδ2 T cells in combination with ZOL would be beneficial in reducing tumour growth in bone and tumour-associated osteolysis, while also limiting the potential for metastatic spread in patients with advanced breast cancer, greatly reducing the morbidity of the disease. However, further studies are required to understand the interactions between the bone micro-environment, cancer cells, and *in vivo* ZOL uptake to optimise a treatment regimen that achieves maximal anti-cancer efficacy.

Acknowledgments

This work was supported by funds from the National Breast Cancer Foundation (NBCF-13-09) and the research fellowships granted to A. Evdokiou by The Hospital Research Foundation (THRF) and Australian Breast Cancer Research (ABCR).

The authors would like to thank Ms Ruth Williams and Dr. Agatha Labrinidis from Adelaide Microscopy at The University of Adelaide for technical assistance with the SkyScan 1076 and related software.

References

1. Howlader, N.Noone, AM.Krapcho, M.Miller, D.Bishop, K.Altekruse, SF.Kosary, CL.Yu, M.Ruhl, J.Tatalovich, Z.Mariotto, A.Lewis, DR.Chen, HS.Feuer, EJ., Cronin, KA., editors. SEER Cancer Statistics Review, 1975–2013. National Cancer Institute; Bethesda, MD: Apr. 2016 based on November 2015 SEER data submission, posted to the SEER web site, http://seer.cancer.gov/csr/1975_2013/
2. Coleman RE, Rubens RD. The clinical course of bone metastases from breast cancer. Br J Cancer. 1987; 55:61–66. [PubMed: 3814476]
3. Coleman RE. Metastatic bone disease: clinical features, pathophysiology and treatment strategies. Cancer Treat Rev. 2001; 27:165–176. [PubMed: 11417967]
4. Mundy GR. Metastasis to bone: causes, consequences and therapeutic opportunities. Nat Rev Cancer. 2002; 2:584–593. [PubMed: 12154351]
5. Roodman GD. Mechanisms of bone metastasis. N Engl J Med. 2004; 350:1655–1664. [PubMed: 15084698]
6. Ross JR, Saunders Y, Edmonds PM, Patel S, Broadley KE, Johnston SR. Systematic review of role of bisphosphonates on skeletal morbidity in meta-static cancer. BMJ. 2003; 327:469. [PubMed: 12946966]

7. Ross JR, Saunders Y, Edmonds PM, Patel S, Wonderling D, Normand C, et al. A systematic review of the role of bisphosphonates in metastatic disease. Health Technol Assess. 2004; 8:1–176.
8. Carding SR, Egan PJ. Gammadelta T cells: functional plasticity and heterogeneity. Nat Rev Immunol. 2002; 2:336–345. [PubMed: 12033739]
9. Ensslin AS, Formby B. Comparison of cytolytic and proliferative activities of human gamma delta and alpha beta T cells from peripheral blood against various human tumor cell lines. J Natl Cancer Inst. 1991; 83:1564–1569. [PubMed: 1683671]
10. Muraro M, Mereuta OM, Carraro F, Madon E, Fagioli F. Osteosarcoma cell line growth inhibition by zoledronate-stimulated effector cells. Cell Immunol. 2007; 249:63–72. [PubMed: 18163982]
11. Li Z, Xu Q, Peng H, Cheng R, Sun Z, Ye Z. IFN-gamma enhances HOS and U2OS cell lines susceptibility to gammadelta T cell-mediated killing through the Fas/Fas ligand pathway. Int Immunopharmacol. 2011; 11:496–503. [PubMed: 21238618]
12. Cui Q, Shibata H, Oda A, Amou H, Nakano A, Yata K, et al. Targeting myeloma-osteoclast interaction with Vgamma9Vdelta2 T cells. Int J Hematol. 2011; 94:63–70. [PubMed: 21698356]
13. Sato K, Kimura S, Segawa H, Yokota A, Matsumoto S, Kuroda J, et al. Cytotoxic effects of gammadelta T cells expanded ex vivo by a third generation bisphosphonate for cancer immunotherapy. Int J Cancer. 2005; 116:94–99. [PubMed: 15756684]
14. Mattarollo SR, Kenna T, Nieda M, Nicol AJ. Chemotherapy and zoledronate sensitize solid tumour cells to Vgamma9Vdelta2 T cell cytotoxicity. Cancer Immunol Immunother. 2007; 56:1285–1297. [PubMed: 17265022]
15. Benzaid I, Monkkonen H, Stresing V, Bonnelye E, Green J, Monkkonen J, et al. High phosphoantigen levels in bisphosphonate-treated human breast tumors promote Vgamma9Vdelta2 T-cell chemotaxis and cytotoxicity in vivo. Cancer Res. 2011; 71:4562–4572. [PubMed: 21646473]
16. Kondo M, Izumi T, Fujieda N, Kondo A, Morishita T, Matsushita H, et al. Expansion of human peripheral blood gammadelta T cells using zoledronate. J Vis Exp. 2011
17. Gober HJ, Kistowska M, Angman L, Jeno P, Mori L, De Libero G. Human T cell receptor gammadelta cells recognize endogenous mevalonate metabolites in tumor cells. J Exp Med. 2003; 197:163–168. [PubMed: 12538656]
18. Poonia B, Pauza CD. Gamma delta T cells from HIV+ donors can be expanded in vitro by zoledronate/interleukin-2 to become cytotoxic effectors for antibody-dependent cellular cytotoxicity. Cytotherapy. 2012; 14:173–181. [PubMed: 22029653]
19. Niu C, Jin H, Li M, Xu J, Xu D, Hu J, et al. In vitro analysis of the proliferative capacity and cytotoxic effects of ex vivo induced natural killer cells, cytokine-induced killer cells, and gamma-delta T cells. BMC Immunol. 2015; 16:61. [PubMed: 26458364]
20. Dieli F, Poccia F, Lipp M, Sireci G, Caccamo N, Di Sano C, et al. Differentiation of effector/memory Vdelta2 T cells and migratory routes in lymph nodes or inflammatory sites. J Exp Med. 2003; 198:391–397. [PubMed: 12900516]
21. D'Asaro M, La Mendola C, Di Liberto D, Orlando V, Todaro M, Spina M, et al. V gamma 9V delta 2 T lymphocytes efficiently recognize and kill zoledronate-sensitized, imatinib-sensitive, and imatinib-resistant chronic myelogenous leukemia cells. J Immunol. 2010; 184:3260–3268. [PubMed: 20154204]
22. Aggarwal R, Lu J, Kanji S, Das M, Joseph M, Lustberg MB, et al. Human Vgamma2Vdelta2 T cells limit breast cancer growth by modulating cell survival-, apoptosis-related molecules and microenvironment in tumors. Int J Cancer. 2013; 133:2133–2144. [PubMed: 23595559]
23. Santolaria T, Robard M, Leger A, Catros V, Bonneville M, Scotet E. Repeated systemic administrations of both aminobisphosphonates and human Vgam-ma9Vdelta2 T cells efficiently control tumor development in vivo. J Immunol. 2013; 191:1993–2000. [PubMed: 23836057]
24. Fisher JP, Heuijerjans J, Yan M, Gustafsson K, Anderson J. Gammadelta T cells for cancer immunotherapy: a systematic review of clinical trials. Oncoimmunology. 2014; 3:e27572. [PubMed: 24734216]
25. Nakazawa T, Nakamura M, Park YS, Motoyama Y, Hironaka Y, Nishimura F, et al. Cytotoxic human peripheral blood-derived gammadeltaT cells kill glioblastoma cell lines: implications for

cell-based immunotherapy for patients with glioblastoma. J Neurooncol. 2014; 116:31–39. [PubMed: 24062140]

26. Kobayashi H, Tanaka Y, Yagi J, Minato N, Tanabe K. Phase I/II study of adoptive transfer of gammadelta T cells in combination with zoledronic acid and IL-2 to patients with advanced renal cell carcinoma, Cancer Immunol. Immunother. 2011; 60:1075–1084.
27. Wada I, Matsushita H, Noji S, Mori K, Yamashita H, Nomura S, et al. Intraperitoneal injection of in vitro expanded Vgamma9Vdelta2 T cells together with zoledronate for the treatment of malignant ascites due to gastric cancer. Cancer Med. 2014; 3:362–375. [PubMed: 24515916]
28. Nicol AJ, Tokuyama H, Mattarollo SR, Hagi T, Suzuki K, Yokokawa K, et al. Clinical evaluation of autologous gamma delta T cell-based immunotherapy for metastatic solid tumours. Br J Cancer. 2011; 105:778–786. [PubMed: 21847128]
29. Kalyan, S., He, W., Kabelitz, D. Bone cancer: primary bone cancers and bone metastases. In: Heymann, D., editor. Bone cancer: Primary Bone Cancers and Bone Metastases. Elsevier; 2014. p. 629-636.
30. Zinonos I, Labrinidis A, Lee M, Liapis V, Hay S, Ponomarev V, et al. Apomab, a fully human agonistic antibody to DR5, exhibits potent antitumor activity against primary and metastatic breast cancer. Mol Cancer Ther. 2009; 8:2969–2980. [PubMed: 19808976]
31. Liapis V, Labrinidis A, Zinonos I, Hay S, Ponomarev V, Panagopoulos V, et al. Hypoxia-activated pro-drug TH-302 exhibits potent tumor suppressive activity and cooperates with chemotherapy against osteosarcoma. Cancer Lett. 2015; 357:160–169. [PubMed: 25444931]
32. Beck BH, Kim HG, Kim H, Samuel S, Liu Z, Shrestha R, et al. Adoptively transferred ex vivo expanded gammadelta-T cells mediate in vivo antitumor activity in preclinical mouse models of breast cancer. Breast Cancer Res Treat. 2010; 122:135–144. [PubMed: 19763820]
33. Thaile M, Labrinidis A, Hay S, Liapis V, Bouralexis S, Welldon K, et al. Apo2l/Tumor necrosis factor-related apoptosis-inducing ligand prevents breast cancer-induced bone destruction in a mouse model. Cancer Res. 2006; 66:5363–5370. [PubMed: 16707463]
34. Coxon FP, Thompson K, Roelofs AJ, Ebetino FH, Rogers MJ. Visualizing mineral binding and uptake of bisphosphonate by osteoclasts and non-resorbing cells. Bone. 2008; 42:848–860. [PubMed: 18325866]
35. Liu Z, Eltoum IE, Guo B, Beck BH, Cloud GA, Lopez RD. Protective immunosurveillance and therapeutic antitumor activity of gammadelta T cells demonstrated in a mouse model of prostate cancer. J Immunol. 2008; 180:6044–6053. [PubMed: 18424725]
36. Junankar S, Shay G, Jurczyluk J, Ali N, Down J, Pocock N, et al. Real-time intravital imaging establishes tumor-associated macrophages as the extraskeletal target of bisphosphonate action in cancer. Cancer Discov. 2014
37. Thompson K, Rogers MJ, Coxon FP, Crockett JC. Cytosolic entry of bisphosphonate drugs requires acidification of vesicles after fluid-phase endocytosis. Mol Pharmacol. 2006; 69:1624–1632. [PubMed: 16501031]
38. Roelofs AJ, Coxon FP, Ebetino FH, Lundy MW, Henneman ZJ, Nancollas GH, et al. Fluorescent risedronate analogues reveal bisphosphonate uptake by bone marrow monocytes and localization around osteocytes in vivo. J Bone Miner Res. 2010; 25:606–616. [PubMed: 20422624]
39. Ferrero E, Biswas P, Vettoretto K, Ferrarini M, Uguccioni M, Piali L, et al. Macrophages exposed to Mycobacterium tuberculosis release chemokines able to recruit selected leucocyte subpopulations: focus on gammadelta cells. Immunology. 2003; 108:365–374. [PubMed: 12603603]
40. Horie N, Murata H, Kimura S, Takeshita H, Sakabe T, Matsui T, et al. Combined effects of a third-generation bisphosphonate, zoledronic acid with other anticancer agents against murine osteosarcoma. Br J Cancer. 2007; 96:255–261. [PubMed: 17242698]
41. Koto K, Murata H, Kimura S, Horie N, Matsui T, Nishigaki Y, et al. Zoledronic acid inhibits proliferation of human fibrosarcoma cells with induction of apoptosis, and shows combined effects with other anticancer agents. Oncol Rep. 2010; 24:233–239. [PubMed: 20514467]
42. Fromigue O, Lagneaux L, Body JJ. Bisphosphonates induce breast cancer cell death in vitro. J Bone Miner Res. 2000; 15:2211–2221. [PubMed: 11092402]

43. Boissier S, Ferreras M, Peyruchaud O, Magnetto S, Ebetino FH, Colombel M, et al. Bisphosphonates inhibit breast and prostate carcinoma cell invasion, an early event in the formation of bone metastases. Cancer Res. 2000; 60:2949–2954. [PubMed: 10850442]
44. Montague R, Hart CA, George NJ, Ramani VA, Brown MD, Clarke NW. Differential inhibition of invasion and proliferation by bisphosphonates: anti-metastatic potential of Zoledronic acid in prostate cancer. Eur Urol. 2004; 46:389–401. discussion 401–382. [PubMed: 15306113]
45. Matsumoto S, Kimura S, Segawa H, Kuroda J, Yuasa T, Sato K, et al. Efficacy of the third-generation bisphosphonate, zoledronic acid alone and combined with anti-cancer agents against small cell lung cancer cell lines. Lung Cancer. 2005; 47:31–39. [PubMed: 15603852]
46. Jeong J, Lee KS, Choi YK, Oh YJ, Lee HD. Preventive effects of zoledronic acid on bone metastasis in mice injected with human breast cancer cells. J Korean Med Sci. 2011; 26:1569–1575. [PubMed: 22147993]
47. Ory B, Heymann MF, Kamijo A, Gouin F, Heymann D, Redini F. Zoledronic acid suppresses lung metastases and prolongs overall survival of osteosarcoma-bearing mice. Cancer. 2005; 104:2522–2529. [PubMed: 16270320]
48. Luo KW, Ko CH, Yue GG, Lee MY, Siu WS, Lee JK, et al. Anti-tumor and anti-osteolysis effects of the metronomic use of zoledronic acid in primary and metastatic breast cancer mouse models. Cancer Lett. 2013; 339:42–48. [PubMed: 23896464]
49. Koto K, Horie N, Kimura S, Murata H, Sakabe T, Matsui T, et al. Clinically relevant dose of zoledronic acid inhibits spontaneous lung metastasis in a murine osteosarcoma model. Cancer Lett. 2009; 274:271–278. [PubMed: 18986762]
50. Labrinidis A, Hay S, Liapis V, Ponomarev V, Findlay DM, Evdokiou A. Zoledronic acid inhibits both the osteolytic and osteoblastic components of osteosarcoma lesions in a mouse model. Clin Cancer Res. 2009; 15:3451–3461. [PubMed: 19401351]
51. Labrinidis A, Hay S, Liapis V, Findlay DM, Evdokiou A. Zoledronic acid protects against osteosarcoma-induced bone destruction but lacks efficacy against pulmonary metastases in a syngeneic rat model. Int J Cancer. 2010; 127:345–354. [PubMed: 19924813]
52. Kalyan S, Quabius ES, Wiltfang J, Monig H, Kabelitz D. Can peripheral blood gammadelta T cells predict osteonecrosis of the jaw? An immunological perspective on the adverse drug effects of aminobisphosphonate therapy. J Bone Miner Res. 2013; 28:728–735. [PubMed: 22991330]
53. Pappalardo A, Thompson K. Activated gammadelta T cells inhibit osteoclast differentiation and resorptive activity in vitro. Clin Exp Immunol. 2013; 174:281–291. [PubMed: 23815433]
54. Laggner U, Di Meglio P, Perera GK, Hundhausen C, Lacy KE, Ali N, et al. Identification of a novel proinflammatory human skin-homing Vgamma9V-delta2 T cell subset with a potential role in psoriasis. J Immunol. 2011; 187:2783–2793. [PubMed: 21813772]

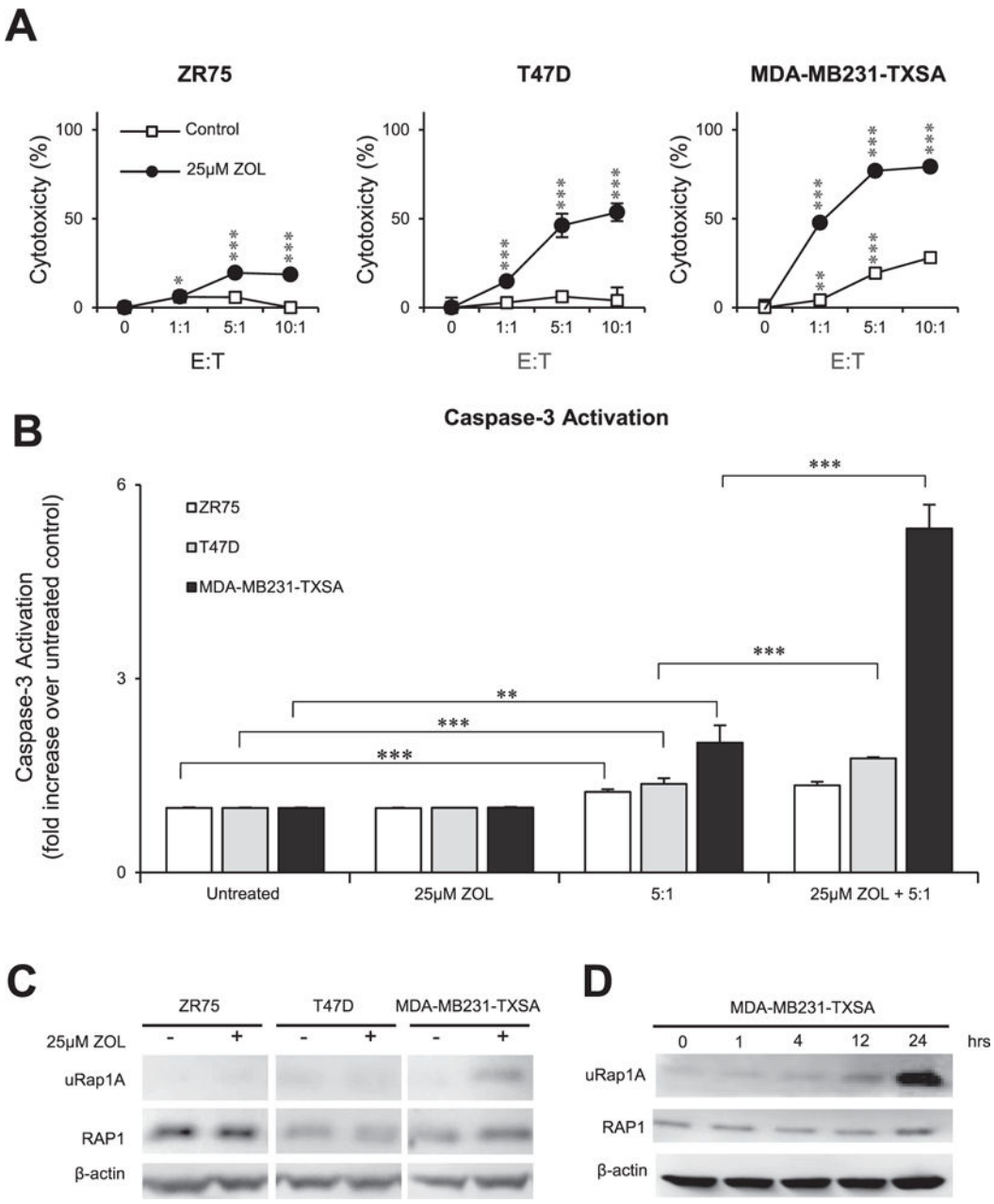

Fig. 1.

ZOL sensitises breast cancer cells to Vγ9Vδ2 T cell cytotoxicity *in vitro*. **A**. ZR75, T47D, and MDA-MB231-TXSA breast cancer cell lines were pre-treated with 25 μM ZOL or left untreated for 24 h. Cancer cells were then co-cultured with *ex vivo* expanded Vγ9Vδ2 T cells (E:T, 1:1, 5:1,10:1). After 9 h, LDH release was measured and expressed as percentage cytotoxicity compared to untreated cells. **B**. Caspase-3 activation of the same cell lines was measured after 24 h pre-treatment with or without 25 μM ZOL, followed by 2 h co-culture with *ex vivo* expanded Vγ9Vδ2 T cells (E:T, 5:1). Caspase-3 activation was expressed as a fold increase over untreated control. For the LDH and Caspase-3 activity assay, data was pooled and normalised from two separate experiments (n = 6). **C**. Western immunoblot

analysis showing inhibition of prenylation in breast cancer cell lines after treatment with or without 25 μM ZOL for 24 h, showing unprenylated RAP1A (uRap1A), total RAP1 protein, and β-actin as loading control. **D**. Western immunoblot analysis showing inhibition of prenylation in MDA-MB231-TXSA treated with 25 μM ZOL over a 24 h time course (0,1, 4,12, 24 h). Images representative of n = 2–3. *p < 0.05, **p < 0.005, ***p < 0.001, ns = non-significant (two-tailed student's t-test, data represent mean ± SEM, n = 3, unless otherwise indicated).

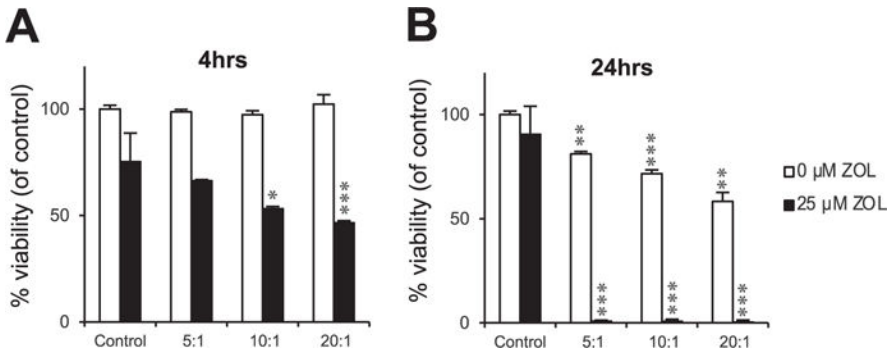

Fig. 2.

Vγ9Vδ2 T cell cytotoxicity against breast cancer cells in vitro occurs in a time dependent manner. Luciferase-tagged MDA-MB231-TXSA breast cancer cells were treated with or without 25 μM ZOL for 24 h. Cancer cells were then co-cultured with *ex vivo* expanded Vγ9Vδ2 T cells (E:T, 5:1,10:1,20:1) for **A**. 4 or **B**. 24 h, and luciferase activity measured and expressed as percentage viability compared to untreated control. Representative data shown from three experiments.*$p < 0.05$, **$p < 0.005$, ***$p < 0.001$, ns = non-significant (two-tailed student's t-test, data represent mean ± SEM, n = 3, unless otherwise indicated).

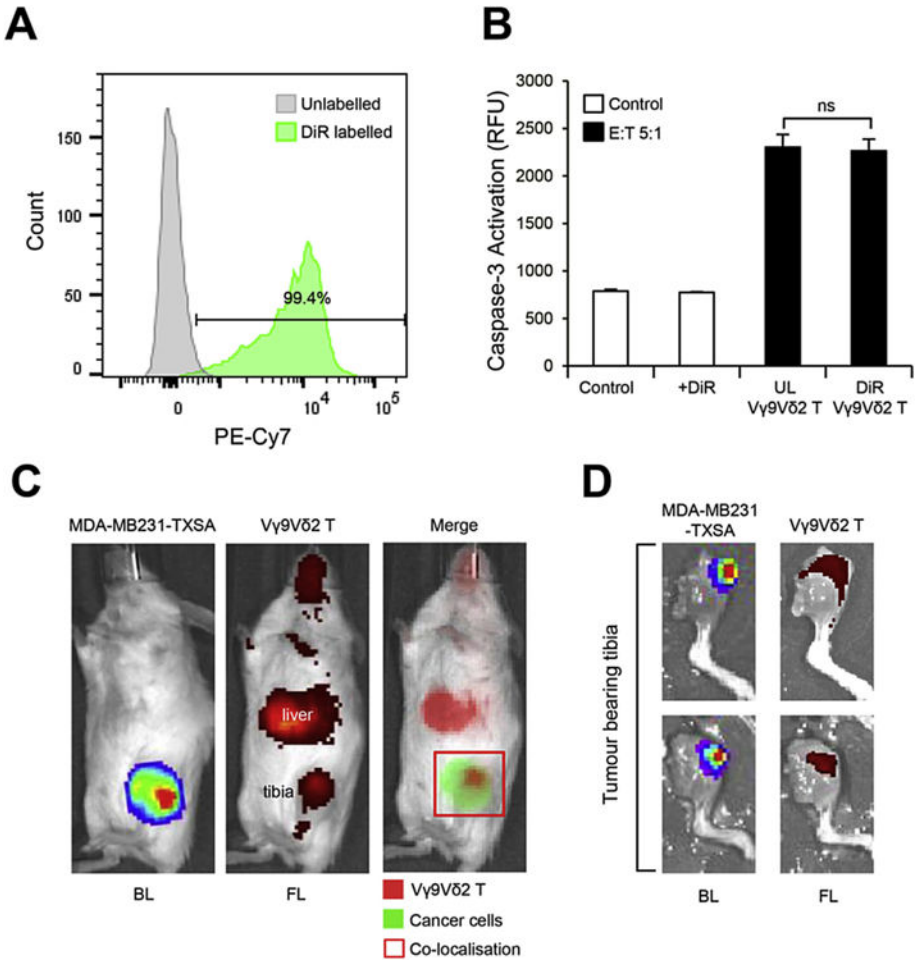

Fig. 3.

Fluorescently labelled Vγ9Vδ2 T cells localise to breast cancer lesions in the bone. *Ex vivo* expanded Vγ9Vδ2 T cells were labelled using DiR dye as outlined in the methods. **A**. Flow cytometric analysis of Vγ9Vδ2 T cell DiR labelling efficacy. **B**. Cytotoxicity of DiR-labelled and unlabelled Vγ9Vδ2 T cells against MDA-MB231-TXSA cancer cells (E:T, 5:1) as shown by caspase-3 activation. **C**. *In vivo* localisation of DiR-labelled Vγ9Vδ2 T cells injected via the tail vein into 5-week old female NOD/SCID mice bearing luciferase-tagged osteolytic breast cancer cells (MDA-MB231-TXSA) in the left tibia. Bioluminescence and fluorescence images were acquired on the IVIS Spectrum *in vivo* imaging system 24 h after infusion and **D**. *ex vivo*, 6 days after infusion (representative images of n = 5). UL = unlabelled, BL = bioluminescence, FL = fluorescence. Percentages shown indicate numbers from lymphocyte population. ns = non-significant (Student's t-test, data represent mean ± SEM, n = 3).

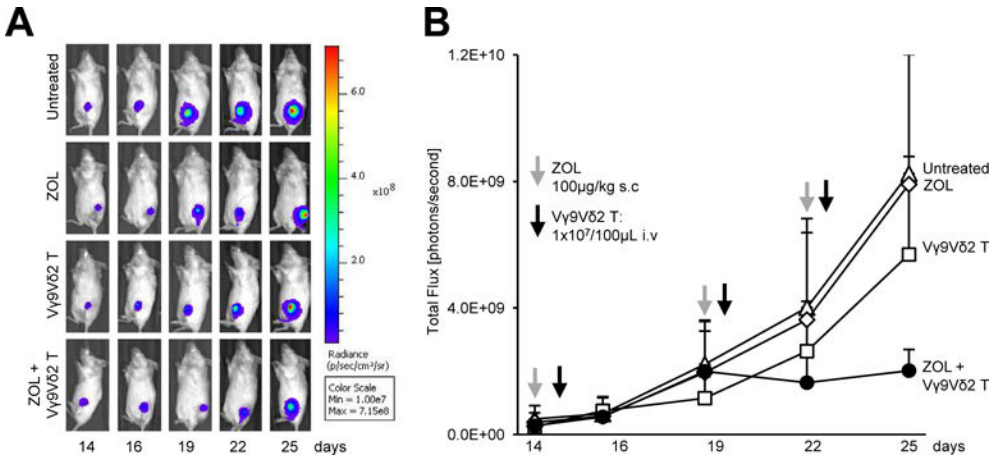

Fig. 4.

ZOL potentiates the anti-cancer efficacy of Vγ9Vδ2 T cells against osteolytic breast cancer. Luciferase-tagged MDA-MB231-TXSA breast cancer cells were injected directly into the left tibial cavity of 5-week old NOD/SCID mice. Once tumours were established, treatments were commenced as outlined in the methods. Whole body bioluminescence images were acquired on the IVIS Spectrum *in vivo* imaging system over the course of the study. **A**. A representative bioluminescence image showing a single mouse from each treatment group over the duration of the study. **B**. The line graph shows the quantification of bioluminescence signal over the course of the study and is expressed as total flux [photons/second] (n = 4–6 mice per group).

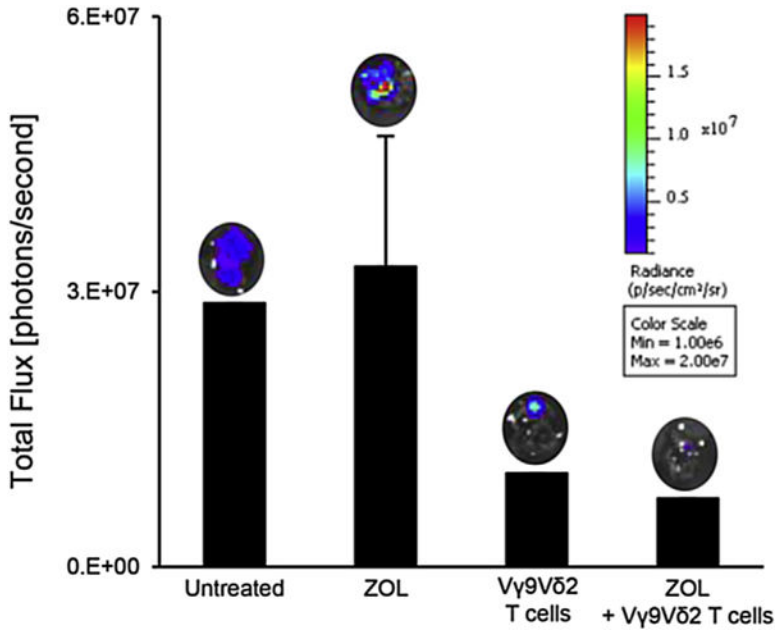

Fig. 5.

Vγ9Vδ2 T cells reduce tumour burden of lung metastases. At the time of sacrifice, lungs were removed for bioluminescence quantification of tumour burden. Bioluminescence signal was detected on the IVIS Spectrum *in vivo* imaging system and is expressed as total flux [photons/second]. A representative bioluminescence image of the lungs from each treatment group is shown.

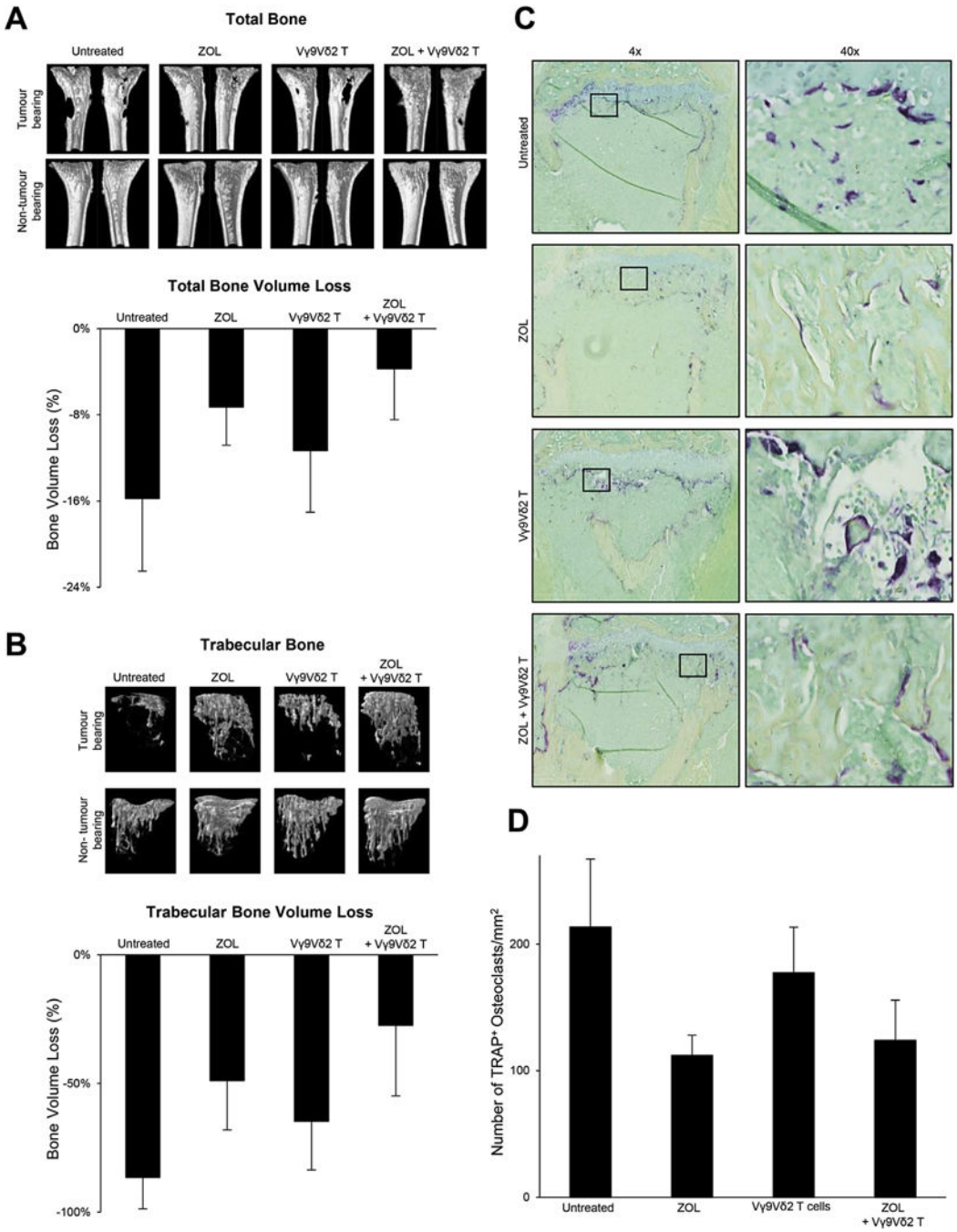

Fig. 6.

Vγ9Vδ2 T cells in combination with ZOL reduce tumour-associated osteolysis in total and trabecular bone. The osteolytic nature of MDA-MB231-TXSA breast cancer cells can be seen in the representative qualitative μCT 3D images and in the quantitative assessment of **A**. total and **B**. trabecular bone. Bone loss percentage is calculated as the percentage difference in bone volume between the tumour bearing and contralateral non-tumour bearing control tibia. **C**. Representative histological sections at 4× and 40 × magnification showing

decalcified tibias from each treatment group stained with TRAP for the detection of osteoclasts. **D**. Quantitative assessment of the number of $TRAP^{+}$ osteoclasts.